DOI: 10.1002/((please add manuscript number))
Article type: Communication

Influence of the Thermodynamic and Kinetic Control of Self-Assembly on the Microstructure Evolution of Silk-Elastin-like Recombinamer Hydrogels

*Arturo Ibáñez-Fonseca[1], Doriana Orbanic[1], Francisco Javier Arias[1], Matilde Alonso[1], Dimitrios I. Zeugolis[2,3], José Carlos Rodríguez-Cabello[1]**

Dr. A. Ibáñez-Fonseca, Dr. D. Orbanic, Prof. F. J. Arias, Prof. M. Alonso, Prof. J. C. Rodríguez-Cabello
[1] BIOFORGE Lab, University of Valladolid – CIBER-BBN. Paseo de Belén 19, 47011 – Valladolid, Spain
E-mail: roca@bioforge.uva.es

Dr. D. I. Zeugolis
[2] Regenerative, Modular & Developmental Engineering Laboratory (REMODEL), Biomedical Sciences Building, National University of Ireland Galway (NUI Galway), Galway, Ireland
[3] Science Foundation Ireland (SFI) Centre for Research in Medical Devices (CÚRAM), Biomedical Sciences Building, National University of Ireland Galway (NUI Galway), Galway, Ireland

Keywords: self-assembly, silk-elastin-like recombinamers, thermodynamics, hydrogels, niches

Abstract

Complex recombinant biomaterials that merge the self-assembling properties of different (poly)peptides provide a powerful tool for the achievement of specific structures, such as hydrogel networks, considering the possibility of tuning the thermodynamics and kinetics of the system through a tailored molecular design. In this work, we combined elastin-like (EL) and silk-like (SL) polypeptides to obtain a silk-elastin-like recombinamer (SELR) with dual self-assembly. First, EL domains force the molecule to undergo a phase transition above a precise temperature, which is driven by entropy and occurs very fast. Then, SL motifs interact through the slow formation of β-sheets, stabilized by H-bonds, creating an energy barrier that opposes phase separation. Both events lead to the development of a dynamic microstructure that evolves over time (growing to a pore size of 49.9 ± 12.7 μm after 1 h), as observed by

live imaging phase contrast microscopy, and to a delayed hydrogel formation (obtained after 2.6 h), as confirmed by rheology. Eventually, the network is arrested due to an increase in β-sheet secondary structures (up to 71.8 ± 0.8%) within SL motifs. This gives a high bond enthalpy that prevents the complete segregation of the SELR from water, which results in a fixed metastable microarchitecture. The resulting porous hydrogels were preliminarily tested as biomimetic niches for the isolation of cells in 3D cultures, showing promising applications in cell biology studies.

Main text

Self-assembled biomaterials have been widely studied over the past few decades with the aim of achieving controlled and well-defined structures, similar to those found in nature, for specific applications.[1] The complexity of self-assembly increases greatly when a combination of (bio)molecules is used to obtain a precise arrangement, but mostly trial and error experiments are needed in order to know which structure is formed from their concomitant self-assembly. Nevertheless, given the current knowledge on the folding of different (poly)peptides,[1b,2] we might be able to obtain specific microstructures built from the combination of peptide "bricks" that can interact mutually. Considering that self-assembly is driven by thermodynamics (enthalpy and entropy) towards a minimum energy or most stable state, and that this process is inherently associated to a particular kinetics, we can achieve an overall control on the self-assembly of polypeptide biohybrids. In this work, we have made use of the recombinant DNA technology to develop a novel silk-elastin-like recombinamer (SELR) that maintains the properties of its constituent polypeptides, namely the Gly-L-Ala-Gly-L-Ala-Gly-L-Ser $(GAGAGS)_n$ hexapeptide repeat from *Bombyx mori* silkworm silk fibroin,[3] and the L-Val-L-Pro-Gly-X-Gly $(VPGXG)_n$ pentapeptide found in natural elastin, where X (the guest residue) can be any amino acid except L-Pro.[4] The silk-

like domains are able to establish strong mutual interactions as they fold into tight *β*-sheets *via* the formation of highly oriented intermolecular hydrogen bonds (H-bonds) within the GAGAGS region, which, thermodynamically, corresponds to a high bond energy or bond enthalpy. This self-assembly process eventually leads to crystallization and thus to an insoluble form of silk. As such, biomaterials comprising this biomolecule possess exceptional strength and have been widely used as threads in clothing and clinics, as well as biomaterials for tissue engineering applications.[5] On the other hand, elastin-like peptides display a thermoresponsive behavior by undergoing an Inverse Temperature Transition (ITT) above the so called transition temperature (T_t), also known as lower critical solution temperature (LCST). The ITT process has been extensively studied for model elastin-like recombinamers (ELRs), and it has been described as the phase separation between water and ELR molecules above the T_t, driven by the difference in the entropy of the system at both temperatures.[6] For instance, below the T_t, water molecules surround hydrophobic residues and form highly ordered clathrate-like structures, which correlates to a low entropy. However, the H-bonds between water molecules that stabilize clathrates break above the T_t, due to the increase in energy, and become disordered bulk water. This results in a higher entropy, which overcomes the enthalpic barrier and leads to a spontaneous phase separation driven by the hydrophobic nature of the ELRs that tend to form thermodynamically stable structures, such as coacervates, *via* self-assembly of the ELR molecules, segregating from water.[7] Given the above, and taking into consideration the different kinetics of self-assembly of elastin-like (EL) and silk-like (SL) recombinamers,[8] we hypothesize that the combination of both structural blocks may lead to a self-assembly initiated by the EL domains through an entropically driven segregation from water. This step will be followed by a thermodynamic halt of the process as a result of the formation of H-bonds between SL motifs, thus resulting in an enthalpic barrier that may ultimately stabilize and strengthen a given structure, such as

the network that conforms a hydrogel. In terms of free energy, this self-assembly process could be defined as a non-equilibrium assembly, meaning that the system will not achieve its potential lower energy, i.e. the one given by the complete phase separation, but it will be kinetically trapped (the changes of the system will be unnoticeable on experimental timescales).[9]

In order to test this hypothesis, we have genetically engineered two different recombinamers, which differ only in the inclusion of SL domains, one being an SELR and the other an ELR. Both comprise the same EL domains, which are based on the combination of lysine and isoleucine-containing pentapeptides (see **Figure S1** in Supporting Information for the schematic representation of both recombinamers and **Table S1** for the complete amino acid sequences), thus showing a slight amphipathicity throughout the whole molecule but still maintaining a strong hydrophobicity due to the burying of lysine-containing pentapeptides within highly hydrophobic isoleucine-containing ones. This experimental setup allowed us to evaluate the role of the SL motifs in the self-assembly. After recombinant bioproduction in *Escherichia coli*, both proteins were characterized by MALDI-TOF mass spectrometry (**Figure S2**), SDS-PAGE (**Figure S3**) and HPLC for the determination of the amino acid composition (**Table S2** and **Table S3**).

Macroscopically, the SELR formed hydrogels at 37 ºC (above the T_t, **Figure S4**) at a concentration of 175 mg mL^{-1}, without expelling water or shrinking, hence maintaining the initial volume of the solution (**Figure 1a**). In contrast, the ELR formed a homotypic coacervate at the same temperature, which segregated from water and eventually sedimented due to the difference in density. To investigate the self-assembly process and formation of the hydrogel by the SELR in further detail, we deposited an 80-μL drop of either the SELR or the ELR in a 96-well tissue culture plate. We then incubated the plate at 37 ºC while performing live imaging with a phase contrast microscope (Nikon Eclipse Ti-E coupled to a Nikon DS-

2MBWc digital camera). This system allowed us to take pictures every 15 seconds for the first 30 minutes for the ELR and for the first hour in the case of the SELR, and every minute for the rest of the experiment for both of them. Interestingly, we observed that the structure formed by the SELR through self-assembly evolved in terms of pore size, thus demonstrating the dynamic nature of the process, which is influenced by the different kinetics of the EL and SL self-assembly (**Figure 1b**, **Video S1**). Conversely, the ELR showed a fast segregation from water (**Video S2**), which, in combination with the macroscopic data, shows that the ELR completely separates from the solvent and does not result in hydrogel formation.

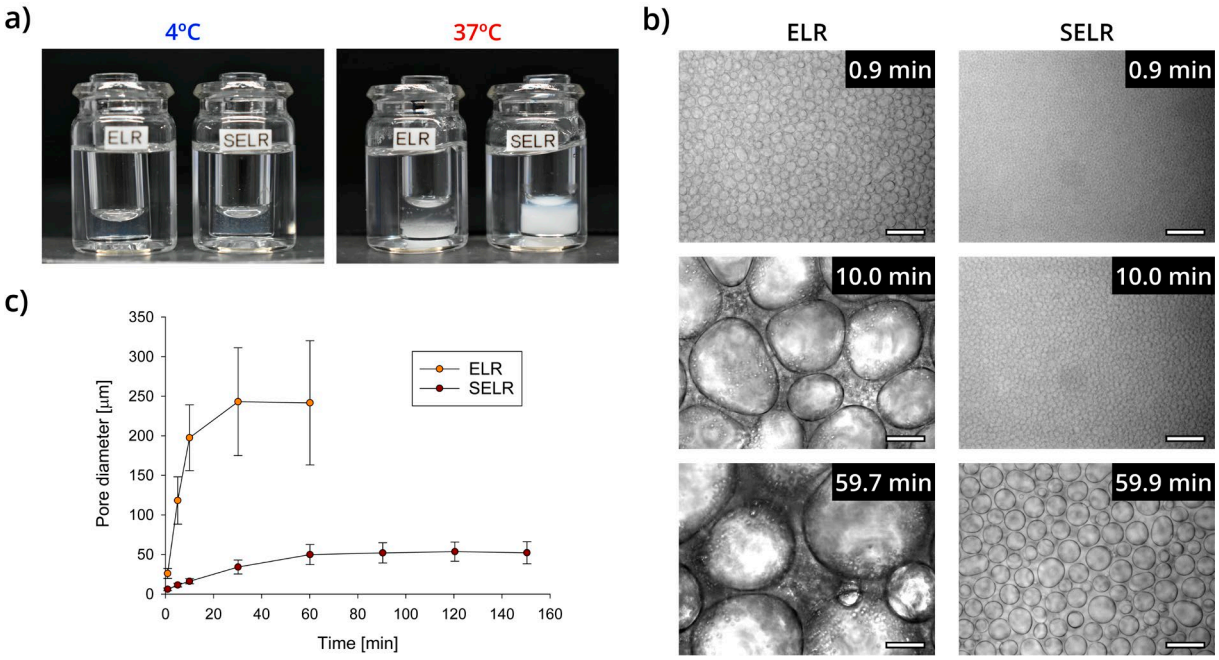

Figure 1. Evaluation of the self-assembly process. a) Macroscopic assessment of the phase separation of the ELR and SELR. Left picture shows the dissolved state of both recombinamers at 4 ºC, while the picture in the right shows the difference in the phase separation between the ELR and the SELR above the T_t (37 ºC). The complete separation of the ELR coacervate can be observed, whereas the SELR maintains the initial volume with the water trapped inside. b) Microscopic study of the evolution of the microstructure of the recombinamers over time at 37 ºC. Phase separation proceeds much faster in the case of the ELR, compared to the SELR that evolves slowly (metastable self-assembly) until complete arrest after approximately 90 minutes. Scale bar = 50 µm. c) Pore diameter at different timepoints, showing the faster dynamics of the ELR (yellow circles) in comparison to the SELR (red circles), which reaches a smaller pore size upon kinetic trapping (n = 3).

We also determined the average pore size at different times, which was 6.1 ± 1.7 μm for the SELR at the onset of hydrogel formation (less than one minute after the transition of the EL domains), subsequently increasing to 49.9 ± 12.7 μm after one hour (**Figure 1c**). In contrast, for the ELR the size increased from 26.0 ± 6.3 μm (0.9 minutes after phase transition) to 243.1 ± 68.1 μm, although these cannot be considered pores, since the structure is not a hydrogel.

In order to study the hydrogel nature of the recombinamers, rheological measurements were performed. In the case of the SELR, the loss modulus (G") was initially higher than the storage modulus (G') (**Figure 2a**), which implies that the sample is a liquid-liquid system rather than a hydrogel at this stage. However, G' increased over time at a higher rate than G", and both moduli eventually crossed after 2.6 h, when the solution became a hydrogel. This time is longer than the one needed to stabilize the hydrogel microstructure, as determined by phase contrast microscopy, suggesting that the phase separation of the SELR from water is stopped by an increase in H-bonds within β-sheets even before a complete hydrogel behavior is observed. However, both techniques have different methodological characteristics, which means that the results obtained in each case might not have a direct correlation. On the other hand, rheology of the ELR shows a higher G" during the whole experiment, meaning that the solution does not become a hydrogel at any point (**Figure 2b**).

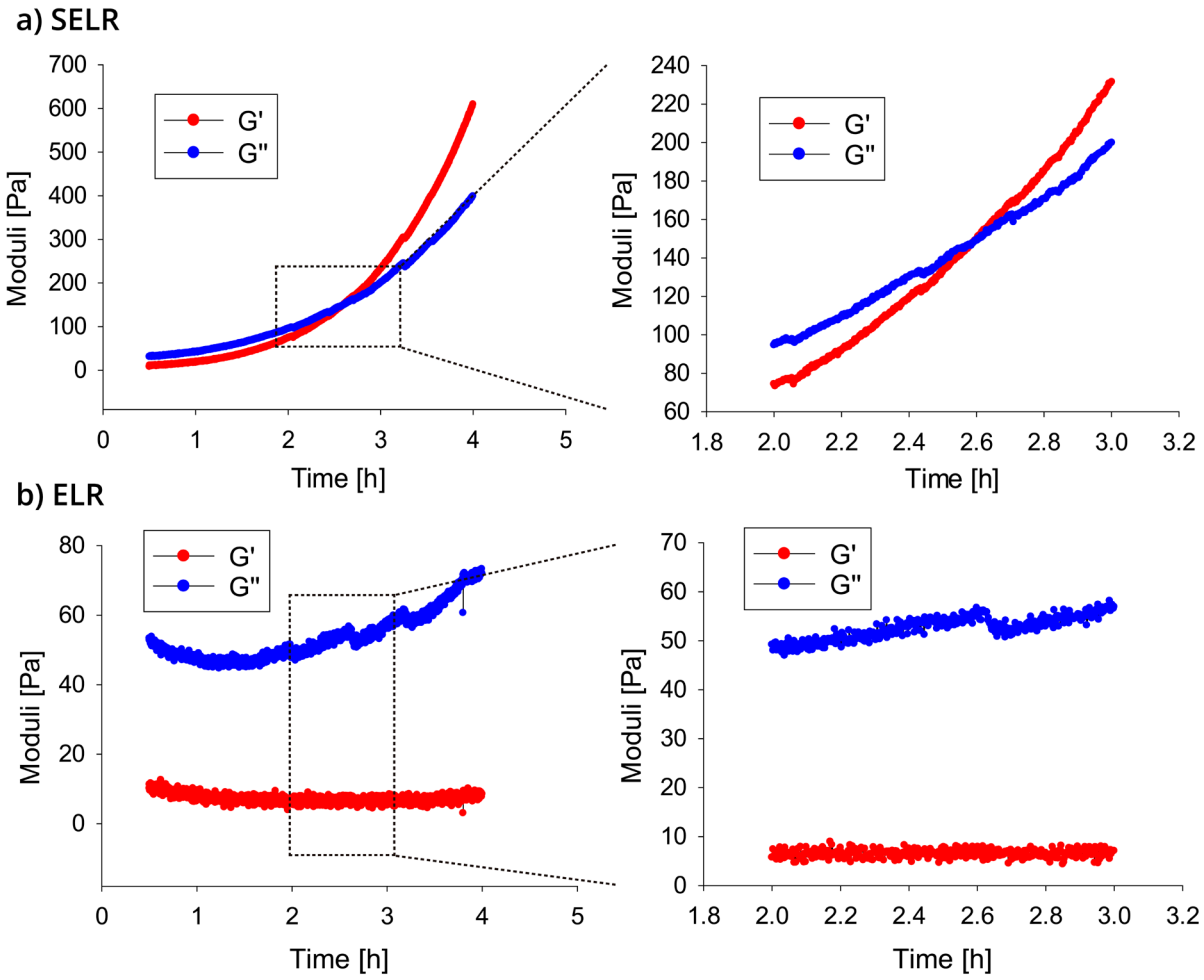

Figure 2. Rheological measurements of the SELR hydrogels (a) and ELR coacervates (b) over time at 37 ºC. The differences can be clearly observed, with an increase in the storage modulus (G', red circles) over time in the case of the SELR, eventually crossing the loss modulus (G", blue circles) after approximately 2.6 h, which implies the formation of a hydrogel. On the other hand, G' for the ELR stays mostly constant at very low values. Small steps can be observed in every graph due to artifacts caused by the addition of solvent (PBS) to avoid sample drying (n = 3).

These observations can be explained considering a number of steps. First, an increase of the temperature above the T_t (LCST) triggers an entropically driven phase separation (ITT), which pushes the system to a new thermodynamic minimum.[1b] This phenomenon has also been described in many other polymer mixtures containing at least one component with a LCST, and it is widely known in polymer science as spinodal decomposition (SD), which is an entropically driven process.[10] Specifically, the separation is forced by the immiscibility between water and EL domains, and proceeds through diffusion once the spinodal curve

(defined as the points at a given temperature and solute concentration at which two phases coexist) has been exceeded (i.e., above the T_t). Therefore, at this early stage, the SELR solution is a liquid-liquid system that comprises water and transitioned SELR molecules (considered as a fluid), which tend to segregate due to thermodynamic instability caused by the difference in density and viscosity between both fluids, and by the overall hydrophobicity of the SELR.[10a] Subsequently, later stages of SD involve a percolation-to-cluster transition, with the water-rich phase forming a droplet-like morphology in order to reduce the interfacial tension/free energy of the system, as it is known that a lower surface area (droplet or sphere) leads to a lower tension/free energy.[11] The confined growth that subsequently takes place leads to an evolution of the microstructure by coarsening, mainly coalescence (driven by diffusion), of the water droplets inside the hydrogel that expel the SELR phase due to the high curvature of the droplet interface.[10a,11a] Finally, these water droplets become trapped in a non-equilibrium stage, thus meaning that they tend to segregate from the hydrogel network but cannot continue the phase separation. This is due to "pinning" or "arrest" of the coarsening of the structure due to gelation,[10a,11a,12] in this case as a consequence of silk annealing or crystallization over time.[8a] Consequently, the whole process could be viewed as a delayed phase separation of SELR and water molecules due to an initial interaction between the SL domains upon EL transition above the T_t, giving a metastable self-assembly.[9] Eventually, the further formation of H-bonds between the β-sheets of SL blocks leads to a complete halt of the self-assembly, thus maintaining the final microstructure of the hydrogel by kinetic trap.[9,13] This strategy for the formation of hydrogels through arrested SD is similar to others described for different polymer mixtures,[14] like a gelatin-water-methanol, where the low temperature acts as quencher,[15] or through glasslike arrest to give colloidal gels.[16]

Regarding similar approaches involving the use of ELRs, Glassman et al. reported the formation of hydrogels as a result of the arrested phase separation of an ELR containing

L-alanine as guest residue, which acts as "arrester" or "pinner", in combination with L-isoleucine.[17] This effect was observed at the nano-scale by small-angle neutron scattering (SANS) and occurs fast enough to avoid coarsening, hence impeding the increase of pore size, and giving nanostructured hydrogels. The use of L-Ala leads to a plastic behavior of the ELR,[18] probably due to the formation of non-covalent bonds other than hydrophobic interactions (e.g. H-bonds), whereas in our case SL domains act as arresters. Moreover, Wang et al. have recently showed how the arrest of ELR molecules through chemical cross-linking impedes the free mobility of the chains and hence influences the self-assembly process.[19] Therefore, the arrest is achieved through the formation of covalent bonds between the molecules, thus preventing phase separation, which, in this case, is the second step of the process. The kinetic control of hydrogel formation is achieved through tuning the cross-linking extent, being another example of formation of a enthalpic barrier to arrest the microstructure and impede the segregation of the ELR from water, although it can be hardly seen as a dynamic process of hydrogel formation, in contrast to our case.

To demonstrate the influence of the SL domains on the stabilization of the hydrogel network and, hence, on the interruption of the phase separation, we performed attenuated total reflection-Fourier transform infrared (ATR-FTIR) spectroscopy analysis on hydrogels freeze-dried at different timepoints after incubation at 37 ºC. We observed that the maximum of the peak corresponding to the amide I band shifted from 1641 to 1631 cm^{-1} after one hour (**Figure 3a**), and eventually shifted further to 1623 cm^{-1} after 72 hours, as a result of the increasing β-sheet content of the hydrogels. The percentage of secondary structures was quantified after spectral deconvolution (**Figure 3b** and **Figure S5**), showing a first increase in total β-sheet (aggregated and non-aggregated) after one hour of incubation at 37 ºC (50.3 ± 1.0%) and a second increase after 72 hours, to 71.8 ± 0.8%. This implies an increase in the bond enthalpy of the SELR-rich phase that forms the hydrogel network, which eventually

results in the creation of an enthalpic barrier that opposes diffusion of water droplets, hence hampering further coalescence and preventing any further hydrogel microstructure reorganization.[12] This also highlights the correlation between the nano- (i.e. formation of H-bonds in *β*-sheets) and the micro-scale (i.e. pore size evolution). Therefore, the increase in *β*-sheet content attributed to the SL domains arrests the system at a metastable energy state; otherwise, phase separation due to EL domains would continue to the most stable state, achieved through the complete segregation of the SELR from water.

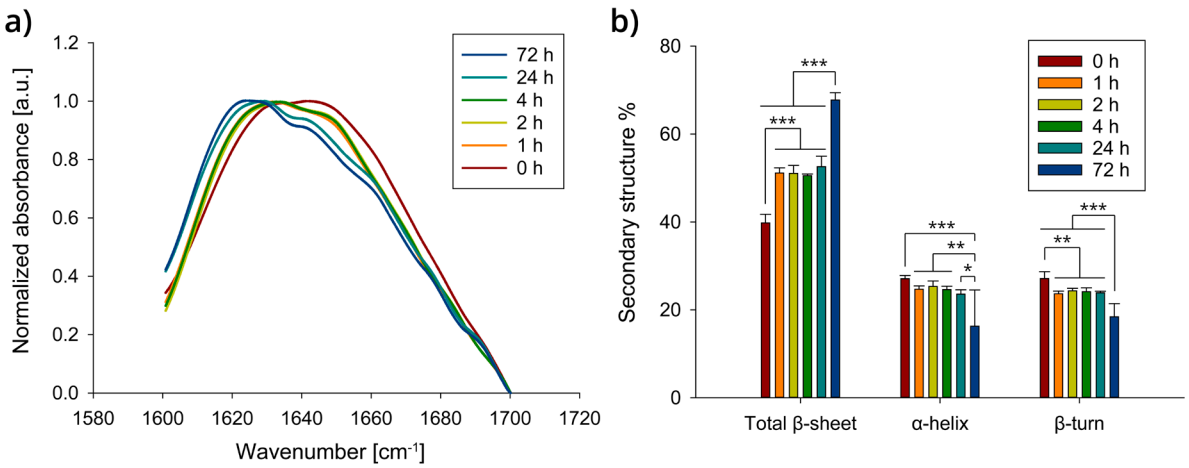

Figure 3. a) ATR-FTIR spectra of the amide I band of the SELR at different timepoints of incubation at 37 ºC showing the shift towards lower wavenumbers with increasing time of incubation, due to *β*-sheet formation between silk domains. b) Percentage of secondary structure in the SELR at different timepoints of incubation at 37 ºC, calculated by spectral deconvolution of the amide I band spectra (*p < 0.05, **p < 0.01 and ***p < 0.001; n = 4).

Some of the first works describing a specific SELR have shown the effect of different concentrations, gelation time and pH, among other parameters, on the physicochemical properties of SELR hydrogels in the context of drug delivery,[20] with special focus on swelling behavior.[21] These articles were followed by others that deepened the knowledge on the self-assembly of SELRs.[22] Nevertheless, none of them stressed how the inherent thermodynamics and kinetics of EL and SL domains drive the overall self-assembly process

when both motifs are combined in a single polypeptide. On the other hand, our group described the concomitant self-assembly of a block co-polymer SELR, highlighting the role of EL motifs in triggering the faster folding of SL domains into *β*-sheets.[8a] However, this work made little emphasis in the influence of the thermodynamics and kinetics of the coordinated self-assembly on hydrogel microstructure. This was, in part, due to the impossibility of studying the process of hydrogel formation through phase contrast microscopy, since the block co-polymer composition of the SELR prevented the complete transition of the molecule above T_t. Moreover, the gelation was almost instantaneous, which precluded the accurate determination of the crossing of G' and G" by rheological analysis. Hence, in that example, the kinetic control on hydrogel microstructure could not be observed so clearly or was non-existent. On the other hand, in our case, the slower kinetics of *β*-sheet formation by SL motifs allowed an evolution of the microstructure towards the formation of pores whose size increases over time, as a result of coarsening, until full thermodynamic arrest. Moreover, this is related to a slow progression of hydrogel formation, as demonstrated by rheological measurements. Therefore, the association of these events with the folding of SL domains into *β*-sheets, suggests that the final hydrogel microstructure, and the dynamics of its evolution, can be tuned by changing the EL/SL ratio in the SELR, which was previously described as a strategy to modulate the mechanical properties (mainly strength and elasticity) of SELR constructs.[23]

Ultimately, the SELR-based hydrogels developed in this work may be used in 3D cell-culture applications since they are able to support cell attachment due to the recombinant inclusion of L-Arg-Gly-L-Asp (RGD) cell-adhesion domains[24] within the SELR molecule. Given the porous microstructure of the hydrogel, cells seeded within it could be isolated as individual cells or clusters of cells. As a preliminary test, human mesenchymal stem cells (hMSCs) were seeded on top of pre-formed SELR hydrogels, incubated at 37 ºC, 10% CO_2, and subsequently

stained for visualization by fluorescence microscopy at different timepoints. As it can be observed (**Figure 4a**), cell number increased homogeneously until full confluence at 30 days, hence meaning that the cells were able to proliferate. For cell encapsulation, the hMSCs were added to a cold 175 mg mL^{-1} SELR solution and hydrogels were formed in 96-well plates, and incubated at 37ºC, 10% CO_2 for 14 days. Then, they were stained for visualization by fluorescence microscopy. We found that cells were well attached to the walls of the pores, arranged individually or as small clusters of cells (**Figure 4b** and **Figure 4c**), thereby supporting the use of these hydrogels for the study of cell behavior in specific controlled conditions. Moreover, Z-stack videos (**Video S3** and **Video S4**, Supporting Information) also show the arrangement of the cells inside the pores, from one edge of the pore to the other. Furthermore, the metabolic activity of the cells increased until day 7, as a result of cell adaptation to the 3D niche and cell proliferation (**Figure 4d**).

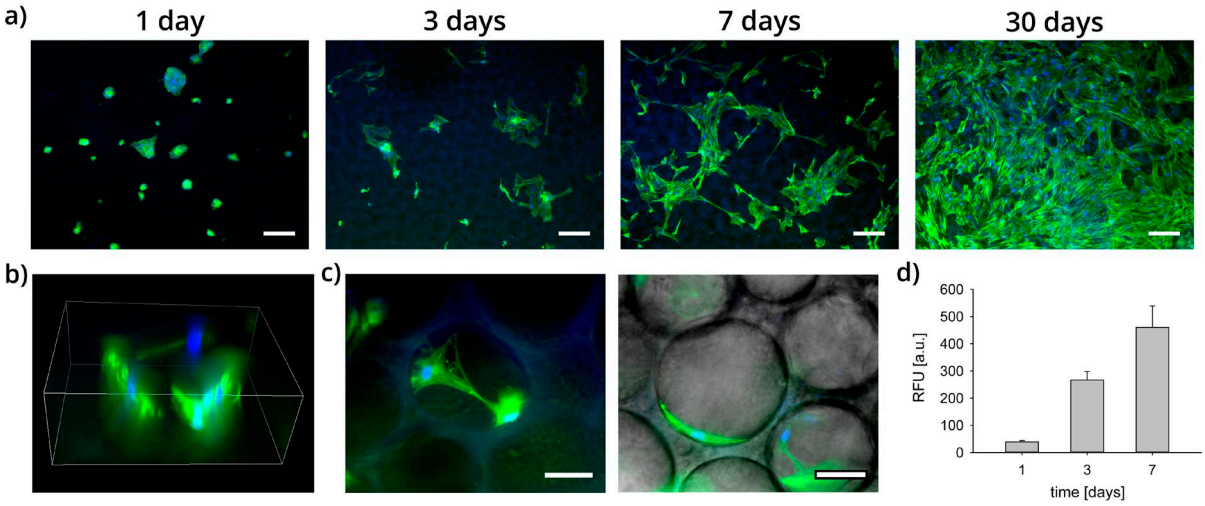

Figure 4. a) Human mesenchymal stem cells (hMSCs) seeded on top of SELR hydrogels and incubated for different timepoints: 1, 3, 7 and 30 days. Actin is stained in green (Phalloidin-Alexa Fluor 488), while nuclei is shown in blue (DAPI). b) 3D projection of hMSCs seeded within SELR hydrogels for 14 days. c) hMSCs attached to the walls of the pores of the SELR hydrogels after 14 days post-seeding. d) Metabolic activity measurement (Alamar Blue) of hMSCs embedded within SELR hydrogels (3D culture) after 1, 3 and 7 days of culture. Scale bar = 100 μm.

In summary, we have designed a novel SELR able to form hydrogels through the dual self-assembly of EL and SL domains, whose different thermodynamics and kinetics influences hydrogel formation. Specifically, the self-assembly is characterized by a rapid phase transition of the EL blocks above the T_t, followed by an initial formation of β-sheets between SL domains, to a low extent, which results in a delayed phase separation of the SELR from water (metastable self-assembly). This leads to a hydrogel microstructure that evolves over time until the complete arrest of the microstructure, as observed in the change in pore size through phase contrast microscopy, due to the tendency of the system to achieve its most stable state, i.e. complete segregation of the SELR from water. As revealed through rheological and FTIR measurements, this occurs in parallel to a gradual strengthening of the network due to further β-sheet folding within SL domains. Finally, the SELR developed in this work could be used as a biomimetic self-assembling system for 3D cell culture, supporting cell attachment through cell adhesion domains. In a preliminary experiment, hMSCs were found isolated within the pores as individual cells or small clusters of cells, which may suggest applications in the formation of controlled niches for the study of cell-cell and cell-biomaterial interactions or the effect of drugs or physical stimuli on isolated cells. Future experiments should focus on the further control of the self-assembly process by modifying the thermodynamics and kinetics through the change of the EL/SL ratio or the environmental conditions (deep of quenching),[22c,25] which may allow the precise spatiotemporal control of the dynamics and of the final microarchitecture of the hydrogel.

Experimental Section

SELR and ELR design and bioproduction

The genetic engineering techniques and heterologous expression of the SELR and the ELR used in this work have been described elsewhere.[26] Briefly, the full-length DNA sequences were obtained using the iterative recursive method via several cloning steps in XL-1 Blue Competent Cells (Agilent Technologies, Inc., CA, USA), then cloned into a pET-25b(+) vector (Novagen, Merck KGaA, Germany) for expression in *Escherichia coli* (BLR(DE3) strain, Novagen, Merck KGaA, Germany). Both the SELR and the ELR were biosynthesized in a 15-L bioreactor (Applikon Biotechnology B.V., Netherlands) and purified by performing several cooling and heating purification cycles (also known as Inverse Transition Cycling) taking advantage of the smart behavior of these recombinamers, which aggregate above their transition temperature. Further centrifugation steps led to a pure product, which was dialyzed against ultra-pure water, filtered through 0.22 μm filters (Nalgene, Thermo Fisher Scientific, MA, USA) to obtain a sterile solution, and freeze-dried prior to storage. Unless otherwise stated, the recombinamers were dissolved in PBS (1.54 mM Potassium Phosphate monobasic (KH_2PO_4), 155.1 mM Sodium Chloride (NaCl), 2.7 mM Sodium Phosphate dibasic (Na_2HPO_4-$7H_2O$); Thermo Fisher Scientific, MA, USA) by incubation during 16-24 h at 4°C for all subsequent analyses. All the experiments were performed in triplicate.

Macroscopic observation of hydrogel formation and sedimentation

For the macroscopic observation of hydrogel formation, 200 μL of recombinamer solution at 175 mg mL^{-1} was deposited in a 1.5 mL glass vial, photographed, and stored at 4°C. Vials were then placed into larger ones (5 mL glass vials) containing warm PBS and incubated on a heating plate (Heidolph MR Hei-Tec, Heidolph, Germany) at 37ºC. Pictures were obtained with a Nikon D3400 camera (Nikon Corporation, Japan).

Microstructure evolution study and pore size determination over time

Live-imaging phase contrast microscopy (Nikon Eclipse Ti-E coupled to a Nikon DS-2MBWc digital camera; Nikon Corporation, Japan) was used to observe the evolution of the hydrogel pore size over time. Thus, 80 μL of either the SELR or the ELR solution was deposited on the bottom of the wells in a 96-well black clear-bottom tissue culture plate (Greiner Bio-One GmbH, Austria). The plate was incubated at 37°C in an incubation chamber on the microscope stage (Okolab S.R.L., Italy) and 150 μL of warm PBS were added to the samples after 5 min to prevent drying. Automated imaging was performed using the NIS-Elements Advanced Research software (version 4.5; Nikon Corporation, Japan), taking images every 15 seconds for the first 30 minutes for the ELR and for the first hour in the case of the SELR, and every minute for the rest of the experiment for both recombinamers. Image analysis was carried out using the Fiji distribution of ImageJ.[27] Pore size over time was determined by measuring at least 30 pores in each image, or all the pores if they were less than 30.

Rheological measurements

Oscillatory rheological measurements were performed to determine the mechanical features of the SELR and ELR solutions using a controlled stress rheometer (AR2000ex, TA Instruments, DE, USA) equipped with a Peltier plate temperature control. To determine the gelation time, a time sweep measurement was performed (1 Hz frequency and 0.5% strain) after deposition of the 175 mg mL^{-1} SELR and ELR solutions between the Peltier (kept at 4°C) and the plate, with a constant gap of 1200 μm. An initial 5 min measurement was performed at 4°C, followed by a long-term (8 h) measurement at 37°C. In order to prevent the samples from drying, they were surrounded by warm PBS.

Evaluation of β-sheet formation within silk domains (ATR-FTIR)

For the analysis of β-sheet formation over time, attenuated total reflectance-Fourier-transform infrared spectroscopy (ATR-FTIR) spectroscopy was performed on freeze-dried SELR-based

hydrogel samples at different time points. Hydrogels were prepared at 175 mg mL^{-1} by depositing 80 μL of the SELR solution on the bottom of 1.5 mL conical tubes. These tubes were then heated to 37°C, and warm PBS was added after 5 min to prevent drying. Samples were taken at different time points (2 min, considered as time 0; 1, 2, 4, 24 and 72 h) and immediately immersed in liquid nitrogen. The frozen hydrogels were freeze-dried and analyzed by ATR-FTIR (Bruker Tensor 27 spectrometer; Bruker Corporation, MA, USA) in the range 450-4000 cm^{-1}, recording 128 scans with a resolution of 2 cm^{-1}. Spectra were obtained using the OPUS spectroscopy software (Bruker Corporation, MA, USA), and further analyzed using Origin 2018 (OriginLab, MA, USA), performing a peak deconvolution in the range of interest (1600-1700 cm^{-1}).[28] Differences in the percentage of secondary structures at different times were statistically analyzed (n = 4) by a one-way ANOVA followed by a pairwise multiple comparison (Holm-Sidak method) in SigmaPlot 14 (Systat Software Inc., CA, USA).

In vitro cell culture

Bone marrow derived human mesenchymal stem cells (hMSCs) were extracted and isolated as described elsewhere,[29] and were generously provided as a gift by Citospin S.L. (Spain). They were cultured for expansion in complete culture medium, namely DMEM low glucose (1 g L^{-1}) (Gibco, USA) supplemented with 10% fetal bovine serum (FBS) (Gibco, USA) and 1% Penicillin/Streptomycin (P/S) (Gibco, USA), at 37 ºC and 10% CO_2. All cells were used at passage 3-5 in subsequent experiments.

As regards cell encapsulation for 3D cell culture, the SELR was dissolved in complete culture medium at 175 mg mL^{-1} (16-24 h, 4ºC) and cells were added to this solution. Then, 40 μL of the resulting mixture was deposited in the wells of 96-well plates and incubated at 37ºC, 10% CO_2. After 15 minutes, warm complete culture medium was added on top of the samples, which were kept in the incubator for 14 days, with medium change every 3 days. After 14

days, the cells inside the hydrogels were fixed with 4% (w/v) paraformaldehyde solution (Sigma-Aldrich, Merck KGaA, Germany) for 10 minutes, and then permeabilized with 0.1% (v/v) Triton X-100 (Sigma-Aldrich, Merck KGaA, Germany) for 5 minutes. The hydrogels were subsequently immersed in a 1:40 dilution of Phalloidin-Alexa Fluor 488 (Invitrogen, Thermo Fisher Scientific, MA, USA) for actin staining during 30 minutes, and, subsequently, in a 300 nM DAPI solution for nuclei staining during 2 minutes. All steps were performed at room temperature.

In order to perform 2D cell cultures, hydrogels were formed prior to cell seeding by depositing 40 μL of the SELR solution (prepared as described above) and incubating at 37ºC, 10% CO_2 for 15 minutes. Then, 2,500 hMSCs were seeded on top of the hydrogels and incubated accordingly. Cells were stained after different timepoints (1, 3, 7 and 30 days), as described above.

For image acquisition, hydrogels were placed on slides and observed with a fluorescence microscope (Nikon Eclipse Ti-E coupled to a Nikon DS-2MBWc digital camera; Nikon Corporation, Japan) at different magnifications. Z-stack videos were obtained using the NIS-Elements Advanced Research software (version 4.5; Nikon Corporation, Japan).

Supporting Information

Supporting Information is available from the Wiley Online Library or from the author.

Acknowledgements

The authors are grateful for the funding from the Spanish Government (MAT2016-78903-R, MAT2016-79435-R, RTI2018-096320-B-C22), Junta de Castilla y León (VA317P18), Interreg V A España Portugal POCTEP (0624_2IQBIONEURO_6_E) and Centro en Red de Medicina Regenerativa y Terapia Celular de Castilla y León. The authors also want to thank Rocío García Lera and Elena Gómez Hernández for the help in the production of the recombinamers.

Received: ((will be filled in by the editorial staff))
Revised: ((will be filled in by the editorial staff))
Published online: ((will be filled in by the editorial staff))

References

[1] a) S. I. Stupp, 1 - Self-assembling biomaterials: Beginnings, recent progress, and the future. In *Self-assembling Biomaterials*, Azevedo, H. S.; da Silva, R. M. P., Eds. Woodhead Publishing: Sawston, Cambridge, UK, 2018; pp 1; b) A. C. Mendes, E. T. Baran, R. L. Reis, H. S. Azevedo, *Wiley Interdiscip. Rev. Nanomed. Nanobiotechnol.* **2013,** *5* (6), 582; c) S. Zhang, *Nature Biotechnology* **2003,** *21*, 1171.

[2] J. Wang, K. Liu, R. Xing, X. Yan, *Chem. Soc. Rev.* **2016,** *45* (20), 5589.

[3] C.-Z. Zhou, F. Confalonieri, M. Jacquet, R. Perasso, Z.-G. Li, J. Janin, *Proteins: Struct., Funct., Bioinf.* **2001,** *44* (2), 119.

[4] J. C. Rodríguez-Cabello, L. Martín, M. Alonso, F. J. Arias, A. M. Testera, *Polymer* **2009,** *50* (22), 5159.

[5] a) J. G. Hardy, L. M. Römer, T. R. Scheibel, *Polymer* **2008,** *49* (20), 4309; b) G. H. Altman, F. Diaz, C. Jakuba, T. Calabro, R. L. Horan, J. Chen, H. Lu, J. Richmond, D. L. Kaplan, *Biomaterials* **2003,** *24* (3), 401; c) N. Dinjaski, D. L. Kaplan, *Current Opinion in Biotechnology* **2016,** *39*, 1; d) W. Huang, A. Rollett, D. L. Kaplan, *Expert Opinion on Drug Delivery* **2015,** *12* (5), 779; e) A. Girotti, D. Orbanic, A. Ibáñez-Fonseca, C. Gonzalez-Obeso, J. C. Rodríguez-Cabello, *Adv. Healthc. Mater.* **2015,** *4* (16), 2423.

[6] D. W. Urry, *Angew. Chem. Int. Ed. Engl.* **1993,** *32* (6), 819.

[7] a) J. C. Rodríguez-Cabello, A. Ibáñez-Fonseca, M. Alonso, L. Poocza, F. Cipriani, I. González de Torre, Elastin-Like Polymers: Properties, Synthesis, and Applications. In *Encyclopedia of Polymer Science and Technology*, 2017; b) A. Ibáñez-Fonseca, T. Flora, S. Acosta, J. C. Rodríguez-Cabello, *Matrix Biology* **2019,** *84*, 111.

[8] a) A. Fernandez-Colino, F. J. Arias, M. Alonso, J. C. Rodriguez-Cabello, *Biomacromolecules* **2014,** *15* (10), 3781; b) Q. Lu, H. Zhu, C. Zhang, F. Zhang, B. Zhang, D. L. Kaplan, *Biomacromolecules* **2012,** *13* (3), 826.

[9] R. K. Grötsch, J. Boekhoven, 11 - Unique properties of supramolecular biomaterials through nonequilibrium self-assembly. In *Self-assembling Biomaterials*, Azevedo, H. S.; da Silva, R. M. P., Eds. Woodhead Publishing: Sawston, Cambridge, UK, 2018; pp 235.

[10] a) D. L. Elbert, *Acta Biomater.* **2011,** *7* (1), 31; b) J. W. Cahn, J. E. Hilliard, *J. Chem. Phys.* **1958,** *28* (2), 258.

[11] a) N. Lorén, A. Altskär, A.-M. Hermansson, *Macromolecules* **2001,** *34* (23), 8117; b) B. Crist, A. R. Nesarikar, *Macromolecules* **1995,** *28* (4), 890; c) D. Chandler, *Nature* **2005,** *437*, 640.

[12] B. Crist, *Macromolecules* **1996,** *29* (22), 7276.

[13] Y. Yan, J. Huang, B. Z. Tang, *Chem. Commun.* **2016,** *52* (80), 11870.

[14] a) R. Bansil, G. Liao, P. Falus, *Physica A: Statistical Mechanics and its Applications* **1996,** *231* (1), 346; b) A. Onuki, S. Puri, *Physical Review E* **1999,** *59* (2), R1331.

[15] a) R. Bansil, Journal de Physique IV Colloque **1993**, 3 (C1), 225; b) R. Bansil, J. Lal, B. L. Carvalho, *Polymer* **1992,** *33* (14), 2961.

[16] a) S. Manley, H. M. Wyss, K. Miyazaki, J. C. Conrad, V. Trappe, L. J. Kaufman, D. R. Reichman, D. A. Weitz, *Physical Review Letters* **2005,** *95* (23), 238302; b) N. Mahmoudi, A. Stradner, *The Journal of Physical Chemistry B* **2015,** *119* (50), 15522.

[17] M. J. Glassman, B. D. Olsen, *Biomacromolecules* **2015,** *16* (12), 3762.

[18] a) D. W. Urry, *What Sustains Life? Consilient Mechanisms for Protein-Based Machines and Materials*. Birkhäuser Boston: Boston (USA), **2006**; b) R. Machado, A. da Costa, V. Sencadas, C. Garcia-Arévalo, C. M. Costa, J. Padrão, A. Gomes, S. Lanceros-Méndez, J. C. Rodríguez-Cabello, M. Casal, *Biomedical Materials* **2013,** *8* (6), 065009.

[19] H. Wang, A. Paul, D. Nguyen, A. Enejder, S. C. Heilshorn, *ACS Appl. Mater. Interfaces* **2018,** *10* (26), 21808.

[20] J. Cappello, J. W. Crissman, M. Crissman, F. A. Ferrari, G. Textor, O. Wallis, J. R. Whitledge, X. Zhou, D. Burman, L. Aukerman, E. R. Stedronsky, *Journal of Controlled Release* **1998,** *53* (1), 105.

[21] A. A. Dinerman, J. Cappello, H. Ghandehari, S. W. Hoag, *Biomaterials* **2002,** *23* (21), 4203.

[22] a) J. Yeo, W. Huang, A. Tarakanova, Y.-W. Zhang, D. L. Kaplan, M. J. Buehler, *Journal of Materials Chemistry B* **2018,** *6* (22), 3727; b) K. J. Isaacson, M. M. Jensen, A. H. Watanabe, B. E. Green, M. A. Correa, J. Cappello, H. Ghandehari, *Macromolecular Bioscience* **2018,** *18* (1), 1700192; c) X.-X. Xia, Q. Xu, X. Hu, G. Qin, D. L. Kaplan, *Biomacromolecules* **2011,** *12* (11), 3844; d) L. D. Muiznieks, F. W. Keeley, *Biopolymers* **2016,** *105* (10), 693.

[23] W. Huang, A. Tarakanova, N. Dinjaski, Q. Wang, X. Xia, Y. Chen, J. Y. Wong, M. J. Buehler, D. L. Kaplan, *Advanced Functional Materials* **2016,** *26* (23), 4113.

[24] E. Ruoslahti, M. D. Pierschbacher, *Cell* **1986,** *44* (4), 517.

[25] M. D. Golinska, T. T. H. Pham, M. W. T. Werten, F. A. de Wolf, M. A. Cohen Stuart, J. van der Gucht, *Biomacromolecules* **2013,** *14* (1), 48.

[26] J. C. Rodriguez-Cabello, A. Girotti, A. Ribeiro, F. J. Arias, *Methods Mol. Biol.* **2012,** *811*, 17.

[27] a) J. Schindelin, I. Arganda-Carreras, E. Frise, V. Kaynig, M. Longair, T. Pietzsch, S. Preibisch, C. Rueden, S. Saalfeld, B. Schmid, J.-Y. Tinevez, D. J. White, V. Hartenstein, K. Eliceiri, P. Tomancak, A. Cardona, *Nat. Methods* **2012,** *9*, 676; b) C. A. Schneider, W. S. Rasband, K. W. Eliceiri, *Nat. Methods* **2012,** *9* (7), 671.

[28] Y. Li, J. C. Rodriguez-Cabello, C. Aparicio, *ACS Appl. Mater. Interfaces* **2017,** *9* (7), 5838.

[29] L. Orozco, A. Munar, R. Soler, M. Alberca, F. Soler, M. Huguet, J. Sentís, A. Sánchez, J. García-Sancho, *Transplantation* **2013,** *95* (12), 1535.

The combination of elastin and silk-like polypeptides leads to a complex self-assembly involving an entropy-driven phase segregation of elastin from water and an increase in enthalpy due to H-bonding between silk domains. The different kinetics of the processes results in a peculiar hydrogel microarchitecture that evolves over time, whose pores act as biomimetic niches for 3D culture of isolated cells.

Self-assembly

A. Ibáñez-Fonseca 1, D. Orbanic 1, F. J. Arias 1, M. Alonso 1, D. I. Zeugolis 2,3, J. C. Rodríguez-Cabello 1*

Influence of the Thermodynamic and Kinetic Control of Self-Assembly on the Microstructure Evolution of Silk-Elastin-like Recombinamer Hydrogels

ToC figure

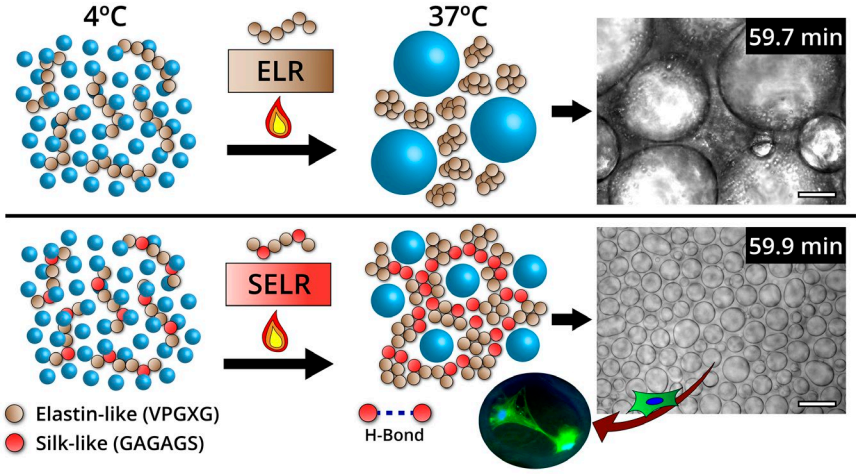

Supporting Information

Influence of the Thermodynamic and Kinetic Control of Self-Assembly on the Microstructure Evolution of Silk-Elastin-like Recombinamer Hydrogels

*Arturo Ibáñez-Fonseca[1], Doriana Orbanic[1], Francisco Javier Arias[1], Matilde Alonso[1], Dimitrios I. Zeugolis[2,3], José Carlos Rodríguez-Cabello[1]**

Dr. A. Ibáñez-Fonseca, D. Orbanic, Prof. F. J. Arias, Prof. M. Alonso, Prof. J. C. Rodríguez-Cabello
[1] BIOFORGE Lab, University of Valladolid – CIBER-BBN. Paseo de Belén 19, 47011 – Valladolid, Spain
E-mail: roca@bioforge.uva.es

Dr. D. I. Zeugolis
[2] Regenerative, Modular and Developmental Engineering Laboratory (REMODEL), Biomedical Sciences Building, National University of Ireland Galway (NUI Galway), Galway, Ireland
[3] Science Foundation Ireland (SFI) Centre for Research in Medical Devices (CÚRAM), Biomedical Sciences Building, National University of Ireland Galway (NUI Galway), Galway, Ireland

Supplementary Experimental Details

Details on the rheological setup

The frequency and strain values used were taken from the literature,[1] and their suitability evaluated by performing frequency sweep and strain sweep measurements using SELR hydrogels formed in situ. First, the mechanical properties of the hydrogel were measured at 37°C and 0.5% strain in the frequency range 0.1-20 Hz. The complex modulus linearity was determined by carrying out a strain sweep mode experiment at 37°C, with a frequency of 1 Hz and in the strain range 0.01-10%.

Transition temperature determination by differential scanning calorimetry (DSC)

Differential scanning calorimetry (DSC) was used to determine the transition temperature of the recombinamers. The solutions were prepared at 50 mg mL^{-1} in PBS and 20 μL of either the SELR or ELR solution was deposited in the aluminum crucible and the measurement was performed using a Mettler Toledo 822e (Mettler Toledo, OH, USA), with PBS as reference.

References

[1] A. Fernandez-Colino, F. J. Arias, M. Alonso, J. C. Rodriguez-Cabello, *Biomacromolecules* **2014**, *15*, 3781.

Supplementary Tables and Figures

Table S1. Abbreviated amino acid sequence and molecular weight of the ELR and SELR used in this work. The sequence corresponding to the elastin-like blocks is represented in blue, while the one for silk-like domains is denoted in green. Cell adhesion domains are shown in red, with the RGD tri-peptide in bold.

	Abbreviated amino acid sequence	Mw (Da)
ELR	MESLLP-$(VGIPG)_{20}$-$([(VPGIG)_2$-VPGKG-$(VPGIG)_2]_2$-AVTG**RGD**SPASS-$[(VPGIG)_2$-VPGKG-$(VPGIG)_2]_2$-$)_6$-$(VGIPG)_{20}$-V	75427
SELR	MESLLP-$(VGIPG)_{20}$-$([(VPGIG)_2$-VPGKG-$(VPGIG)_2]_2$-AVTG**RGD**SPASS-$[(VPGIG)_2$-VPGKG-$(VPGIG)_2]_2$-V$(GAGAGS)_6G)_6$-$(VGIPG)_{20}$-V	88376

Table S2. Comparison between the predicted number of each amino acid and the experimental values for the **ELR** used in this work.

Amino acid	Predicted	Experimental
Asp	6	8.44
Ser	19	18.76
Glu	1	4.91
Gly	332	329.64
Thr	6	7.05
Ala	12	15.49
Pro	167	169.36
Arg	6	7.18
Val	167	165.70
Met	1	1.26
Ile	136	132.97
Leu	2	2.01
Lys	24	16.49
TOTAL	879	879

Table S3. Comparison between the predicted number of each amino acid and the experimental values for the **SELR** used in this work.

Amino acid	Predicted	Experimental
Asp	6	9.14
Ser	49	43.29
Glu	1	2.22
Gly	428	435.25
Thr	6	5.99
Ala	72	72.54
Pro	167	169.18
Arg	6	6.14
Val	173	162.32
Met	1	1.00
Ile	136	139.27
Leu	2	3.92
Lys	24	22.00
TOTAL	1071	1072.26

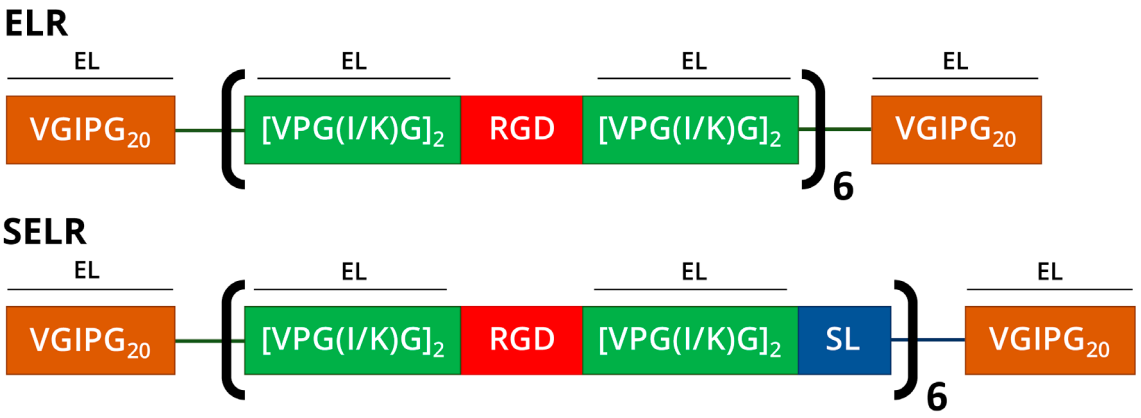

Figure S1. Schematic representation of the ELR and SELR used in this work. SL stands for silk-like, while EL means elastin-like.

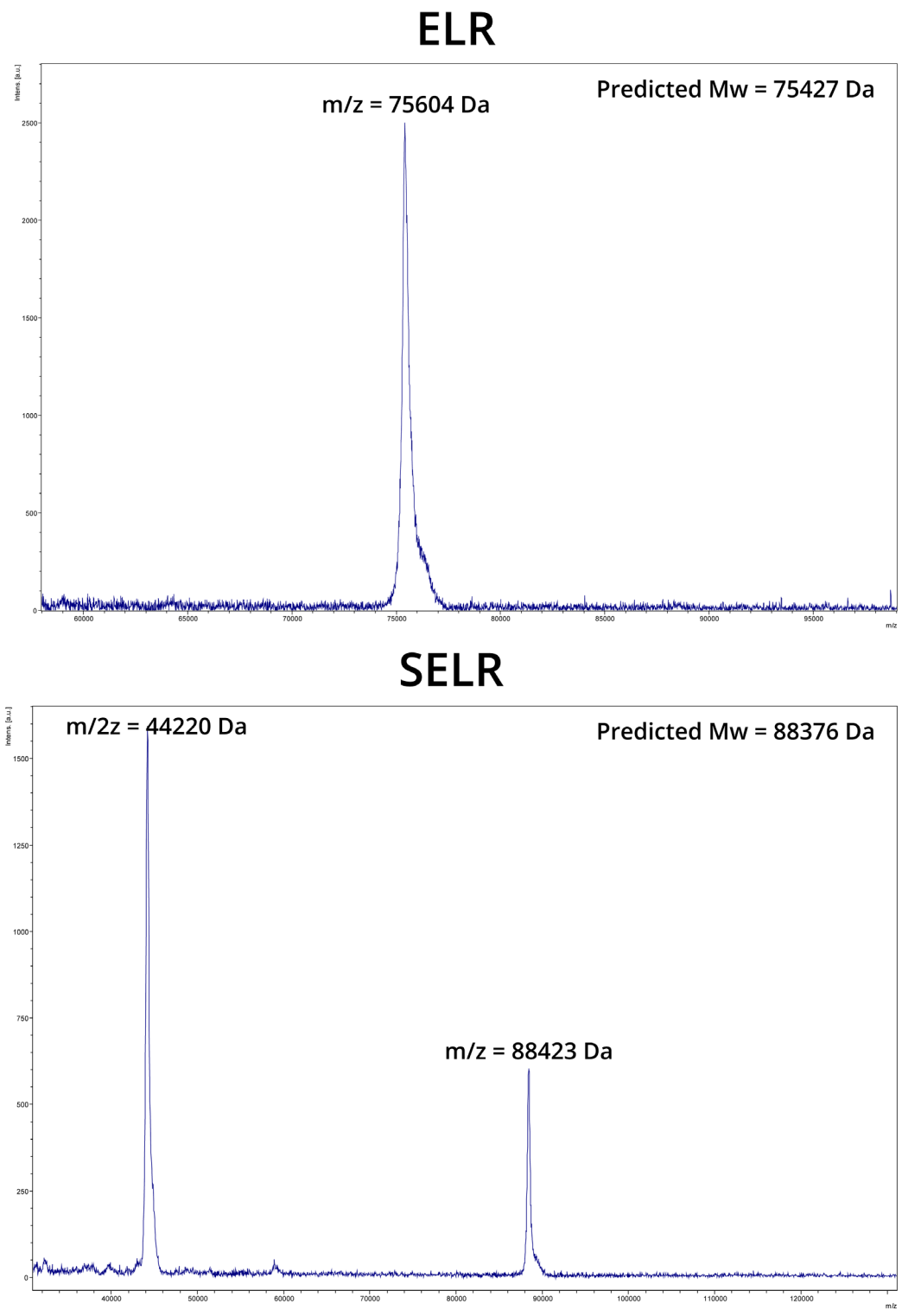

Figure S2. MALDI-TOF spectra of the ELR and SELR, which confirms the agreement between the experimental and the expected *Mw* for both recombinamers. MALDI-TOF spectra represent non-quantitative intensity (a.u.) against m/z (mass divided by net charge of the molecule) of the recombinamers.

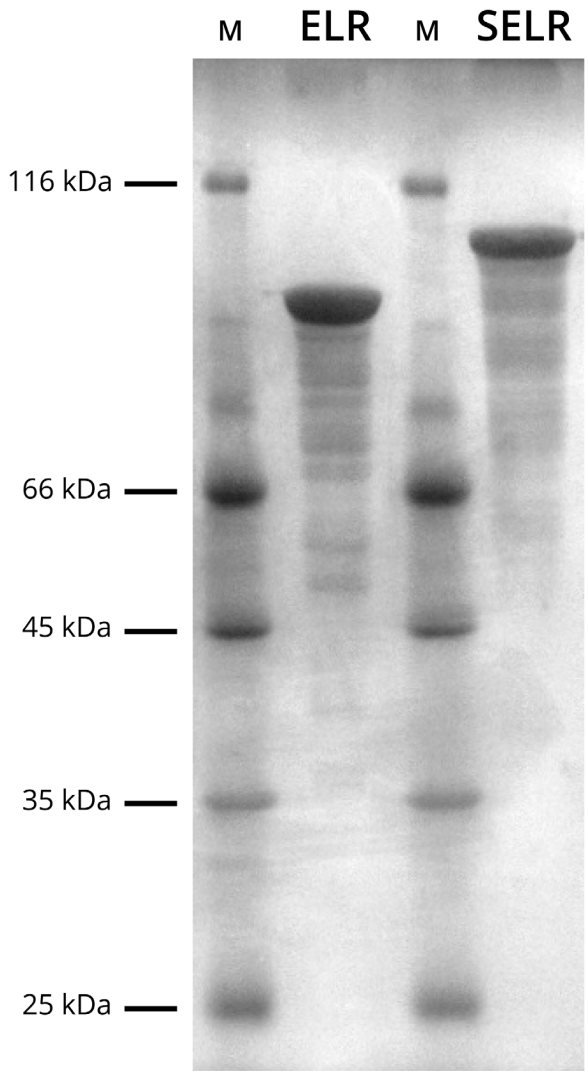

Figure S3. SDS-PAGE of the ELR and SELR dissolved in ultrapure water at 1 mg/mL. The result shows a good correlation between the experimental and the theoretical *Mw*. M: Pierce Unstained Protein MW Marker (Thermo Fisher Scientific, MA, USA).

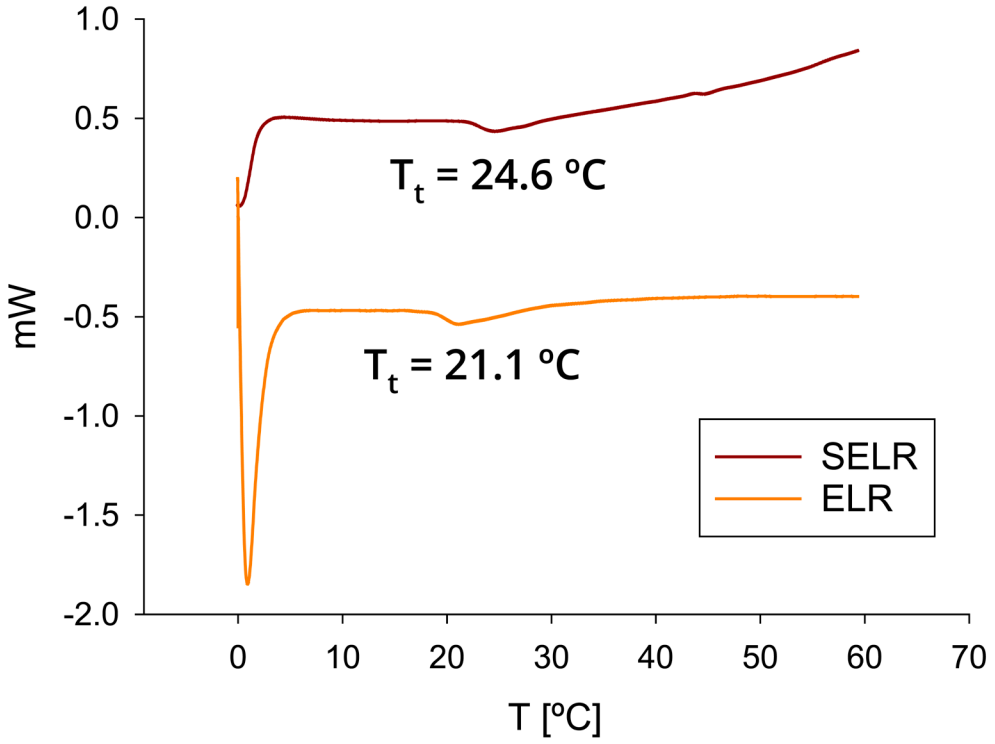

Figure S4. DSC spectra of the ELR and SELR, indicating the T_t at 50 mg mL^{-1} in PBS.

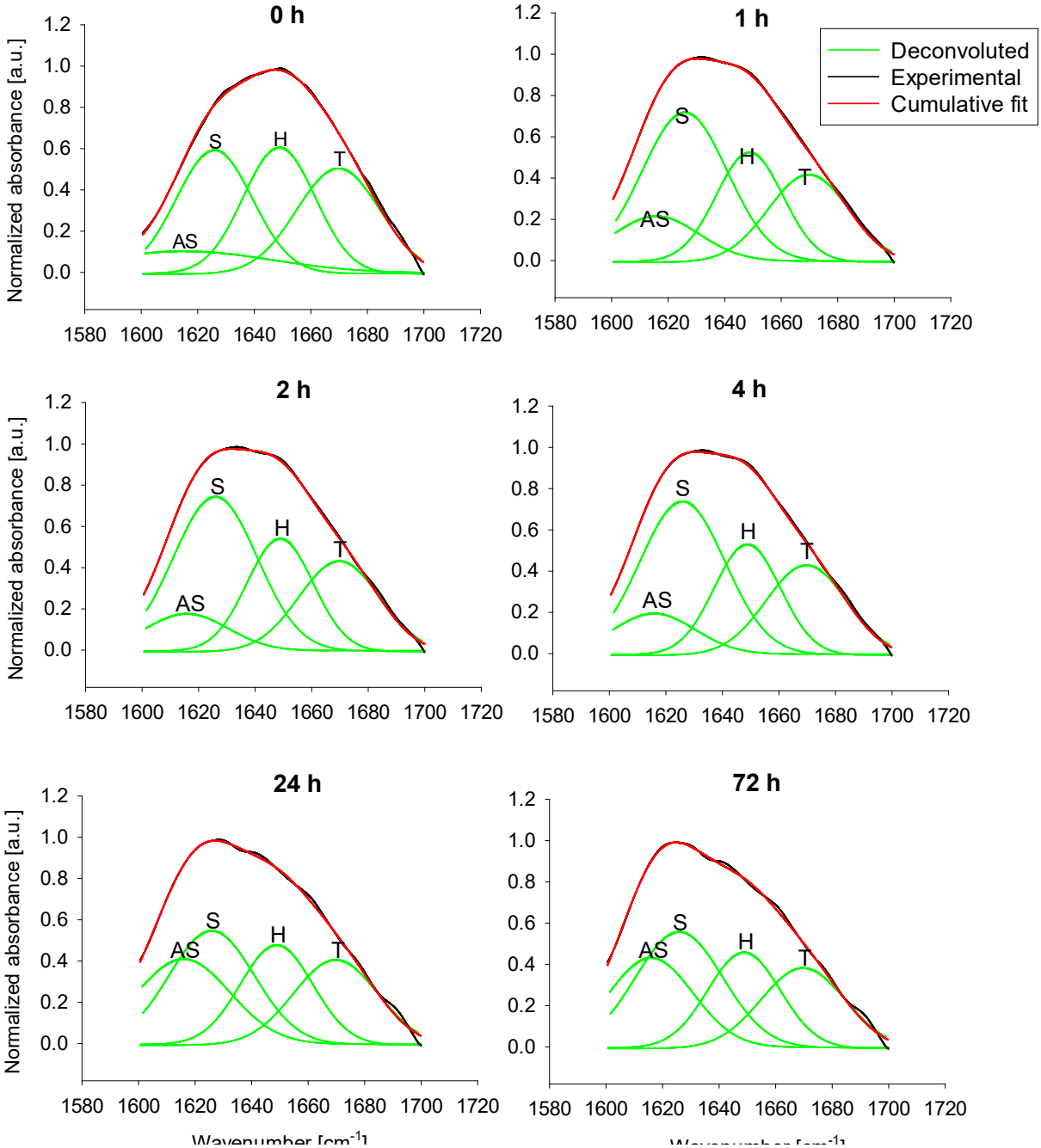

Figure S5. Fourier transform infrared spectroscopy deconvolution for the quantification of protein secondary structure in the SELR. AS: aggregated β-sheet, S: β-sheet, H: α-helix, T: β-turn.

Supplementary Videos

Video S1. Time-lapse video made of live-imaging phase contrast microscopy pictures of a SELR, from time zero (after 5 minutes at 37 ºC) to 4 hours. Pictures were taken every 15 seconds for the first hour and every minute for the rest of the experiment.

Video S2. Time-lapse video made of live-imaging phase contrast microscopy pictures of a ELR, from time zero (after 5 minutes at 37 ºC) to 1 hour. Pictures were taken every 15 seconds for the first 30 minutes and every minute for the rest of the experiment.

Video S3. Z-stack video made of pictures taken at different planes of hMSCs embedded in a SELR hydrogel after 14 days of culture. Actin is stained in green (Phalloidin-Alexa Fluor 488), while nuclei are stained in blue (DAPI). 10X magnification (scale bar = 100 μm).

Video S4. Z-stack video made of pictures taken at different planes of hMSCs embedded in a SELR hydrogel after 14 days of culture. Actin is stained in green (Phalloidin-Alexa Fluor 488), while nuclei are stained in blue (DAPI). 20X magnification (scale bar = 50 μm).